Reeb Graph for Automatic 3D Cephalometry

Mestiri Makram   *mmestiri@gmail.com*
Enit/Electrical/Image Processing
Enit
Elnasr 2, 2037, Tunisia

Hamrouni Kamel   *Hamrouni.kamel@lsts.com*
Enit/Electrical/Image Processing
Enit
Elnasr 2, 2037, Tunisia

Abstract

The purpose of this study is to present a method of three-dimensional computed tomographic (3D-CT) cephalometrics and its use to study cranio/maxilla-facial malformations. We propose a system for automatic localization of cephalometric landmarks using reeb graphs. Volumetric images of a patient were reconstructed into 3D mesh. The proposed method is carried out in three steps: we begin by applying 3d mesh skull simplification, this mesh was reconstructed from a head volumetric medical image, and then we extract a reeb graph. Reeb graph mesh extraction represents a skeleton composed in a number of nodes and arcs. We are interested in the node position; we noted that some reeb nodes could be considered as cephalometric landmarks under specific conditions. The third step is to identify these nodes automatically by using elastic mesh registration using "thin plate" transformation and clustering. Preliminary results show a landmarks recognition rate of more than 90%, very close to the manually provided landmarks positions made by a medical stuff.

Keywords: Reeb Graph, Cephalometry Landmarks, Thin Plate, LCP.

1. INTRODUCTION

Radiographic cephalometry has been one of the most important diagnostic tools in maxillofacial diseases, since its introduction in the early 1930. It deals with the morphological scientific study of the dimensions of all the structures present in a human head, usually through the use of standardized lateral head radiographs. Generations of doctors have relied on the interpretation of these images for their diagnosis and treatment planning as well as for the long-term follow-up of growth and treatment results. Also in the planning for surgical orthodontic corrections of jaw discrepancies, lateral/antero-posterior cephalograms have been valuable tools.

Parameters measurement is based on a set of agreed upon feature point's landmarks. The detection of the landmarks plays an essential role in diagnosis and treatment planning by doctors. Head-growing analyzing with anatomical landmarks was first proposed by Arc Thomson, in 1917 [1]. His approach was based on a deforming grid. Changes in the landmarks position resulted in deformations of the grid. His method was applied not only to quantify the effects of growth, but also to relate different individuals and even different species. A malocclusion is a misalignment of teeth or incorrect relation between the teeth of the two dental arches, Broadbent [2] and later Brodie [3] applied a method based in landmarks to quantify malocclusions and study their effects.

They used radio-graph image to define the Landmarks, head structure like bony or soft tissue, had to be identified. This approach was used for measurement specification at an individual of known age, sex and race to quantify head anatomy differences for diagnosis, such as the one shown in Figure 1.
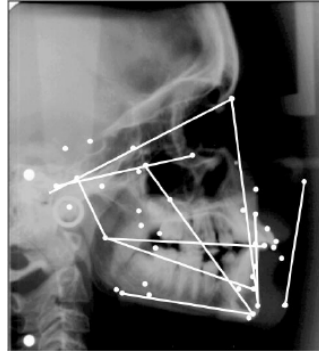
FIGURE 1: Manual Extraction of Cephalometry Landmarks in X-ray Image.

Downs [4] proposed in 1948 the first cephalometric analysis method. His approach was based on measurements of 10 angles from a lateral radiographs from a group of selected individuals; he calculates the average values and gives them a clinical significance. His approach was the basis for most methods used at present.

Ricketts [5] and Steiner [6] proposed traced lines between significant landmarks, so their length and angles can be measured and compared with standard values shown in Figure 2.
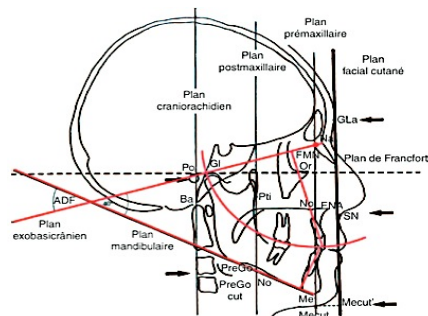
FIGURE 2: Line Traced Between Significant Landmarks [6].

Locating landmarks depends on medical expertise to locate the landmarks manually. This can take an experienced orthodontist up to 30 min. The process is time consuming, subject to human error and tedious.

An automated system would help to eliminate the above-mentioned problems and hence produce repeatable results.

2. RELATED WORKS
All the automatic cephalometric landmarks recognition methods use 2D image processing, the various methods used by researchers in this field found in the literature can be divided into three different approaches: knowledge-based feature detection, pattern matching and neural networks with fuzzy inference system.

Levy [7] proposed in 1986 the first automatic extraction of cephalometric landmarks. His method was based on knowledge based line extraction technique. He begins with applying median filter and histogram equalization to enhance the X-rays images, then he applies a Mero-Vassy operator [8] to extract relevant edges using knowledge-based line tracker. The landmarks are then located according to their geometric definition online crossing. This method requires good X-rays image (cannot be guaranteed in practice). Parthasaraty [9] proposed an enhancement of levy approach by introducing a multi resolution pyramidal analysis of X-rays images to reduce the processing time.

Yen [10], Contereras [11], Jackson [12], Cohen [13] and Davis and Forsyth [14] presented similar knowledge-based edge tracking methods. These methods depend highly on X-ray image quality and can be used only for landmarks located on an edge.

The second approache used mathematical or statistical models to narrow down the search area for each landmark, and then shape-matching techniques are used to locate the exact location of each landmark. Cardillo and Sid-Ahmed [15] proposed a method based on a combination of mathematical modeling methods, like affine transformation to remove the shifts, rotations and size differences to reduce the size of the search area. Then, they applied a shape recognition algorithm based on gray-scale mathematical morphology to locate the landmarks. The method locates 76% of the landmarks within 2 mm. Grauetal[16], adds a line detection module to select the most significant lines in Sid-Ahmed[15] approach. Then, he applies mathematical morphology transformations for shape recognition. The disadvantage of theses methods is that it's very sensitive to noise present in X-rays images. Desvignes [17] proposed a statistical method based on estimation of landmarks locations using adaptive coordinate space where locations are registered. The method was tested on a set of 58 X-rays, of which 28 were used for training. They obtain 99.5% of the landmarks but with 4:5 mm mean error between the real position and the estimated position, far from the authorized range (±2 mm). Hutton [18] used active shape models for cephalometric landmarking. They established a template of possible deformations from a training set of hand-annotated image. The result was 35% of 16 landmarks within an acceptable range of ±2 mm. Implementation could be used as a first estimation location of the landmarks.

The third category of researchers used neural networks and fuzzy inference systems to locate the landmarks. Uchino [19] proposed a fuzzy learning machine that could learn the relation between the gray levels of the image and the location of the landmarks. They begin by dividing the image into nine blocks, each one is an input to the fuzzy learning machine. The weights were adjusted by learning the coordinates of the landmark. The block containing the landmark was divided in nine separate blocks until landmark location is obtained. This method produced an average error of 2:3 mm. this method depends highly on scale, rotation and shift of X-rays images. Innes [20] highlights regions containing craniofacial features using Pulse Coupled Neural Networks (PCNN) from X-rays images. They get 36.7% rate for the region containing sella landmark, 88.1% for the region containing the chin landamark, and 93.6% for the region containing the nose landmark. The most disadvantage of PCNN's method is that they require a considerable manual contribution to set the required parameters.

In this paper, we are interested in the extension of 2D X-rays to 3D image cephalometry analysis. Some work has been carried out to study the potential advantages of 3D imaging methods, such as computed tomography for cephalometric analysis. Kragskov [21] made a comparative result, using human dry skulls. Ferrario [22] studied 3D facial morphometry using infrared cameras, but only as a supplement for classic cephalometry.

We propose a novel method based on the use of reeb graph for Automatic localization of craniofacial landmarks. The task is a difficult one due to the complexity and variability of cephalometry landmarks.

3.   PROPOSED METHOD

As seen in previous works, many researchers have attempted automatic cephalometric landmarks detections. However, a major drawback of the existing techniques is that they use a 2D representation of a 3D structure. In this paper we are interested in a 3D cephalometric landmarks. The development of spiral CT and cone beam CT has revolutionized the medical image techniques, the former providing outstanding resolution and the latter, with its low cost, allowing unique accessibility, as a result 3-D imaging has become an essential tool in planning and managing the treatment of facial deformity.
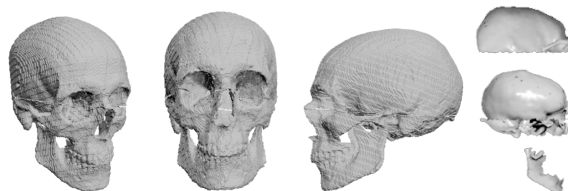
3.1 3D Mesh Database

The image data-base in composed of Dicom images stored in a series of 2D grey level images from a Spiral CT scan (with 512 x 512 matrixes, 110 kV, and 80 mAs) performed at 1 mm slice thickness. The extraction of hard and soft head tissue (bones and skin) is done by using a threshold and region growing technique. Each bones and skin parts are separately constructed using marching cube algorithm as shown in Figure 3.
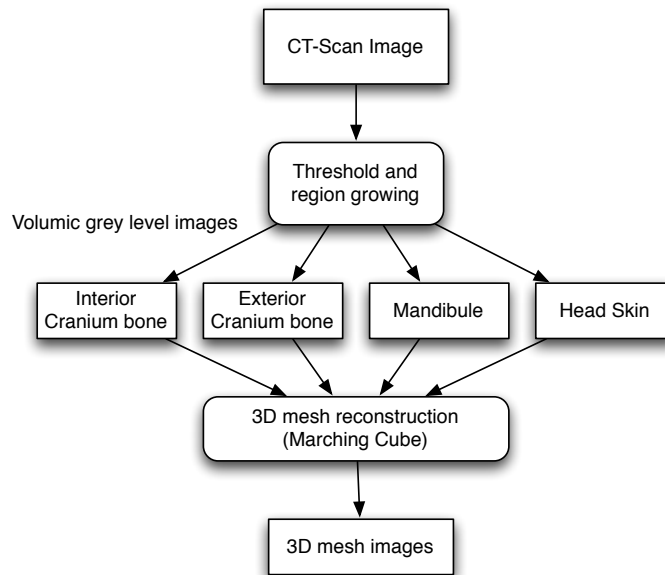
FIGURE 3: 3D Mesh Extraction of Hard and Soft Tissues.

The results of this extraction method are 3 meshes: interior/exterior skull bones, and mandibular bone Figure-4.

**FIGURE 4:** 3D Mesh Extraction from Volumetric CT-Scan .

3.2 3D Cephalometric Landmarks

After getting the mesh database, 3D cephalometric landmarks must be localized in hard tissue. In the literature we found 20 hard landmarks, some of them are presented in table-1.

No	Abbreviation	Hard Tissue
1	N	*Nasion is the midpoint of the frontonasal suture*
2	S	*Sella is the centre of the hypophyseal fossa (sella turcica).*
3	Po	*Porion is the most superior point of each external acoustic meatus.*
4	Or	*Orbitale is the most inferior point of each infra- orbital rim.*
5	ANS	*Anterior Nasal Spine is the most anterior midpoint of the anterior nasal spine of the maxilla.*
6	PNS	*Posterior Nasal Spine is the most posterior midpoint of the posterior nasal spine of the palatine bone.*
7	PMP	*Posterior Maxillary Point is the point of maximum concavity of the posterior border of the palatine bone in the horizontal plane at both sides.*
8	UI	*Upper Incisor is the most mesial point of the tip of the crown of each upper central incisor.*
9	LI	*Lower Incisor is the most mesial point of the tip of the crown of each lower central incisor.*
10	UMcusp	*Upper Molar cusp is the most inferior point of the mesial cusp of the crown of each first upper molar in the profile plane.*

TABLE 1: 10 of the 20 Cephalometric Landmarks Proposed by Swennen [23].

Figure 5 shows some sample of CT-scan images with located landmarks [23].
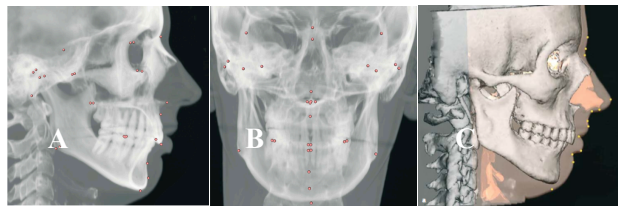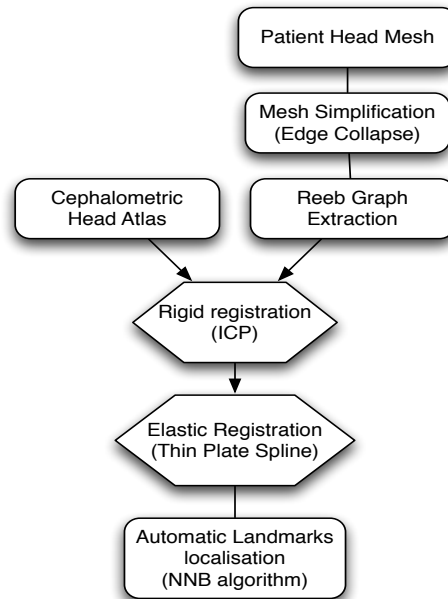

FIGURE 5: A: Right hard cephalometric landmarks, B: Facial hard cephalometric landmarks, C: Soft cephalometric landmarks.

### 3.3 Automatic Localization of Craniofacial Landmarks
Figure 6 presented the bloc diagram of the proposed method for automatic localization of 3D cephalometric landmarks.

After transforming the volumetric medical images to a 3D surface mesh, we need to make a reference shape model containing all cephalometric landmarks information's. This is made with what is called "cephalometric head atlas".

FIGURE 6: Automatic localization of 3D cephalometric landmarks using reeb graphs.

To automatically identify 3D landmarks, we need to have prior knowledge information's. We create a cephalometric head atlas based on medical stuff help. This atlas is composed of skull and skin meshes with 3D cephalometric landmarks as shown in Figure 7.

A　　　　　**B**　　　　　**C**
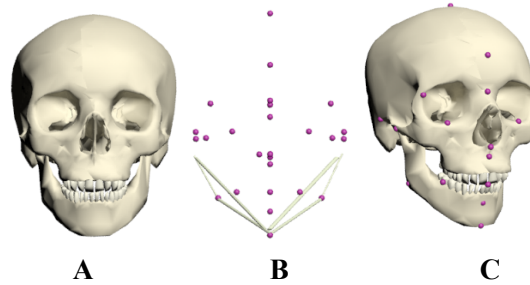
FIGURE 7: Cephalometric atlas of skull. A: initial clean skull mesh, B: Cephalometric landmarks and C: Manual localization of cephalometric landmarks.

In our method we choose to automatically localize cephalometric landmarks using reeb graph. Below we will expose the reeb graph extraction.

The Reeb graph is a chart of connectivity on a surface between its critical points. The main advantage of the reeb graph is that it makes it possible to represent 3D anatomy in a simple topology way. It is composed of nodes and arcs; each whole of level associates a node. The graph of Reeb is obtained starting from the computation of a μ function introduced by the theory of Morse [24] defined on the closed surface of an object in its critical points [25].

We define μ: S $\rightarrow$ R defined on surface S of a 3D object. The Reeb graph is a space quotient of the graph of μ in S, defined by the relation of following equivalence between X ϵ S and Y ϵ S:

$$X \sim Y \Leftrightarrow \begin{array}{l} \cdot\ \mu(X)=\mu(Y) \hspace{2cm} (1) \\ \cdot\ \text{X et Y are in the same Related component of} \\ \mu\text{-1}(\mu(X)),\ \text{and the image } \mu(Y)\ \text{is S.} \end{array}$$

The aspect of the graph is entirely related to the choice of the μ function, which determine the properties of stability and invariance of the resulting graphs. Several functions of application were proposed in the state of the art for the construction of Reeb graphs [26]. One example is the function ($\mu(v(x,y,z)) = z / v \epsilon S$), adapted well for the models whose points are mainly distributed in the Z-axis direction.
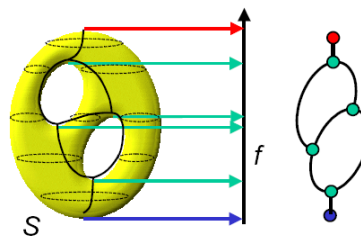
FIGURE 8: Reeb Graph with a z Projection μ Function.

The function suggested in [27] as «outdistances geodesic extrema of curve » is based on growth of areas starting from local Gaussian curves on tops (germs). The results depend on the position of the germs and require no disturbed data; it's a precise calculation of the local curves. Hilaga [27] defines a function by computing the distance from a point of the surface to the center of mass G of the object:

$$(\mu(v) = d(G, v) / v \; \epsilon \; S \; et \; d : Euclidian \; distance) \quad (2)$$

The function defined by Thierny[28] at the characteristic points and the geodesic distances is defined by the following equation:

$$\mu(v) = 1 - \delta\left(v, v_p\right) \quad (3)$$

$$With \; \delta\left(v, v_p\right) = \min_{vf_i \epsilon F} \delta(v, v_{f_i})$$

Where δ is the function of the geodesic distances and v_p are characteristic points. The function suggested in [29] is the integral of the geodetic distances $g(v, p)$ of v to the other point's p of the surface (4).

$$\mu(v) \quad = \int_{p \epsilon S} g(v, p) dS. \quad (4)$$

In our approach we choose this μ function and tested it with different mesh simplification. Figure-9 shows an example of reeb graph extraction.
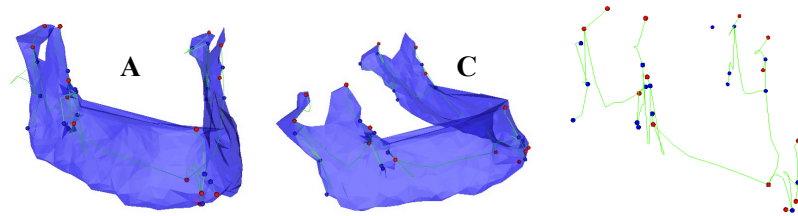

FIGURE 9: A: Mandibule Patient Mesh, B: Reeb Graph Extraction.

Surface mesh simplification is the process of reducing the faces number used in the mesh surface, while keeping preserved as much as possible the overall shape, volume and boundaries. Cignoni [29] proposed a comparison of mesh simplification algorithms, and divided these methods into 7 approaches: coplanar facets merging, controlled vertex/edge/face decimation, re-tiling, energy function optimization, vertex clustering, wavelet-based approaches, and simplification via intermediate hierarchical representation.

We test many simplification methods with reeb graph transformation, and we choose to use the edge collapse method. These techniques reduce a model's complexity by repeated use of the simple edge collapse operation. Researchers have proposed various methods of determining the "minimal cost edge" to collapse at each step (figure-10).
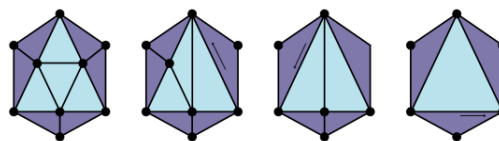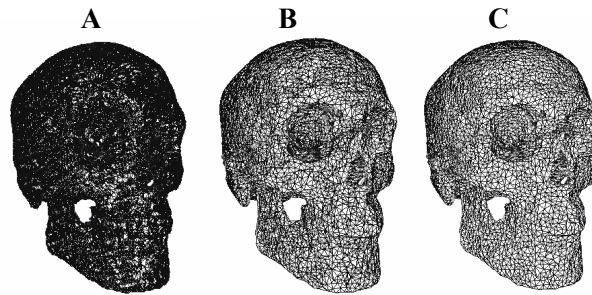

FIGURE 10: Edge Collapse Algorithm [30].

We try to define the effect of the edge collapse simplification process on the reeb graph extraction. The result in shown in figure-11

FIGURE 11: Patient Skull Simplification. A: 332.932 vertices and 662.564 faces, B: 20.047 vertices and 38.958 faces and C: 3.887 vertices and 7320 faces.

We notice that, after mesh simplification, the number of nodes in the reeb graph decreased and they became closed to cephalometric landmarks. And, of course, the computation time is reduced Figure-12.
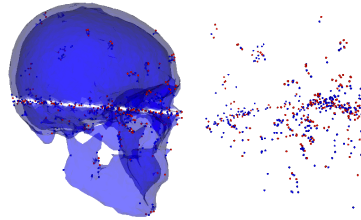
FIGURE 12: Decrease of reeb graph nodes and reconciliation with cephalometric lanmarks.

Mesh registration is a technique used to find a transformation for mapping a source mesh known as a reference mesh and a target mesh. This technique associated to a head cephalometric atlas should help us to get closer to cephalometric landmarks. Every elastic registration process should begin with a rigid one. In this study, we targeted the rigid registration between two different meshes using the ICP algorithm (Iterative Closest Point).

The principle of ICP is to iterate between a step of mapping data and another step of optimization of rigid transformation until convergence. The transformation used for registration is composed of a 3D rotation and translation. At each iteration, the Algorithm provides a list of matched points and an estimate of the transformation. The algorithm converges when the error in distance between matched points is less than a given threshold. The ICP algorithm is presented in the following [30] where Np is the number of points CP1 and CP2 and k is the index of current iteration. Figure-13 shows a example of rigid registration between mesh patient and cephalometric mesh atlas.
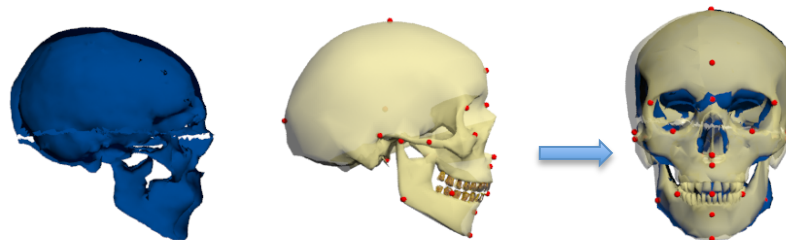
FIGURE 13: Rigid registration between patient and the cephalometric atlas

Mesh elastic registration is a mesh deformation process; one of the transformations that are able to represent elastic deformations is the thin-plate spline (TPS). Thin plate splines were introduced by Bookstein[31] for geometric design. In 2D images, the TPS model describes the transformed coordinates (xT,yT) both independently as a function(7) of the original coordinates (x, y):

(xT,yT)=(fx(x,y),fy(x,y))   (7)

The algorithm begins with a given displacements of a number of landmark points, the TPS model interpolates those points, while maintaining maximal smoothness. For each landmark point (x,y), the displacement is represented by an additional z-coordinate, and, for each point, the thin plate is fixed at position (x, y, z). The strain energy is calculated by integrating the second derivative over the entire surface that can be minimized by solving a set of linear equations.

$$\iint_{R2}\left(\left(\frac{\partial^2 z}{\partial x^2}\right)^2 + 2\left(\frac{\partial^2 z}{\partial x \partial y}\right)^2 + \left(\frac{\partial^2 z}{\partial y^2}\right)^2\right)dxdy \qquad (8)$$

The TPS model for one of the transformed coordinates is given by parameter vectors a and D (9):

$$F(xT,yT)= a1+a2x+a3y+\ldots+$$
$$\sum_{i=1}^{n} D_i F\big(\lVert L_i - (x,y)\rVert\big) \qquad (9)$$

Where F(r)= r2log(r) is the basis function, a = [a1 a2 a3 a4]T defines the affine part of the transformation, D gives an additional non-linear deformation, and the Li are the landmarks that the TPS interpolates figure-4.
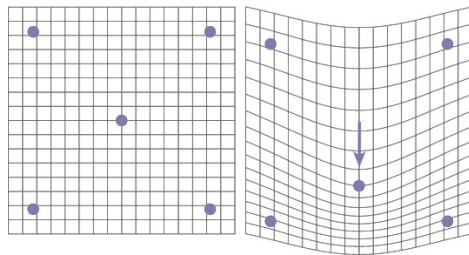
FIGURE 14: A template configuration (left) and a target configuration (right) of five landmarks each.

The deformation right grid illustrates the thin-plate spline function between these configurations as applied to the left regular grid.

The method interpolates some of the points using smoother transformation controlled by a parameter μ, which weights the optimization of landmark distance and smoothness. For $\mu = 0$, there is full interpolation, while for very large μ, there is only an affine transformation. In our methods the landmarks used in the TPS algorithm are the reeb graph nodes as shown in figure-15.
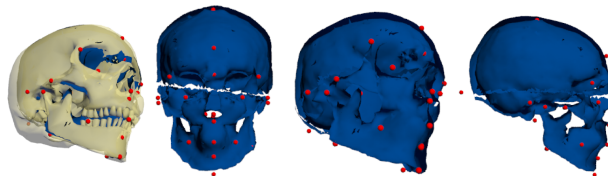

FIGURE 15: Elastic Registration using Thin Plate.

As result of the elastic registration, the patient reeb graph nodes become closer to the atlas cephalometric head landmarks. Since, some reeb graph nodes are not cephalometric landmarks, we have to select the real ones.

Automatic localization of cephalometry landmarks

This step starts with the creation of possible landmark localization in cephalometric atlas. Then, it identifies the reeb graph nodes that exist in the mesh patient. For each node, it searches the closest landmarks in the cephalometric atlas through the calculation of Euclidean distance between an acceptable range of ±2 mm. Finally, as a result all patient reeb graph nodes are associated to a nearest cephalometric landmarks[32].
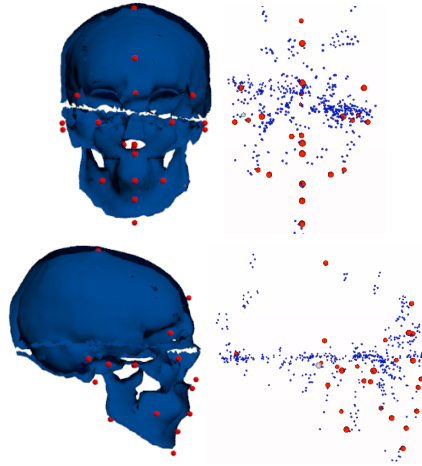
**FIGURE 16:** Localization of Cephalometric Landmarks in Patient Skull.

4.   TEST AND RESULTS

To validate our approach we asked a doctor to conduct manually a cephalometric analysis on the mesh patient. We then calculate the error between its points and cephalometric landmarks automatically localized by our method. The result is showed in the following table:

No	Abbreviation	Error in mm	Recognized
1	N	0.5	Yes
2	S	2.6	No
3	Po	1.3	Yes
4	Or	0.4	Yes
5	ANS	0.7	Yes
6	PNS	2.8	No
7	PMP	2	Yes
8	UI	1.3	Yes
9	LI	1.7	Yes
10	UMcusp	1.8	Yes
11	LMcusp	0.9	Yes
12	Men	0.8	Yes
13	Go	1.5	Yes
14	Fz	1.7	Yes
15	Zy	0.3	Yes
16	A	0.4	Yes
17	B	0.5	Yes
18	Pog	0.8	Yes
19	Ba	0.6	Yes
20	Co	1.4	Yes

TABLE 2: Result of cephalometric landmarks detection

Our method localized 18 landmarks on 20. This mean a percentage of 90% landmarks in patient mesh was recognized.
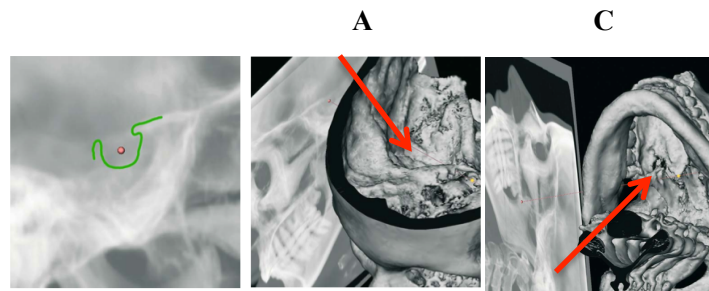
FIGURE 17: Localization of A- Sella and B- PNS Landmarks.

The Sella landmark (S) is very difficult to be localized. It is not localized in the surface mesh, and the doctors need to insert it taking into account the interior skull surface. The Posterior Nasal Spine Landmark (PNS) is defined on the exo-cranial skull base view of the 3-D hard tissue surface representation. This landmark depends highly on the accuracy of the mesh reconstruction.

5. CONCLUSION

In this paper, we have proposed a novel method for automatic 3D localization of cephalometric landmarks. Our approach is based on reeb graph nodes. In particular, we have presented results for localized 90% of cephalometric landmarks in CT-Scan medical images. We initiated a new approach for automatic three-dimensional cephalometric analysis. The proposed method needs to be validated on a larger database.

6. REFERENCES

[1] A.Thomson « On growth and form ». Cambridge, UK: Cambridge Univ. Press, 1992.

[2] Broadbent HB. « A new X-ray technique and its application to orthodontia ». Angle Orthod 1931;

[3] Brodie AG. « On the growth pattern of the human head from the third month to the eighth year of life ». Am J Anat 1941; 68:209–62.

[4] Downs WB. « Variations in facial relationships: their significance in treatment and prognosis ».Am J Orthod 1948; 34:812–40.

[5] Ricketts RM. « Cephalometric Analysis and Synthesis ». Angle Or- thod, 1961; 31:141–56.

[6] Steiner C. « Cephalometrics in clinical practice ». Angle Orthod 1959; 29:8–29.

[7] A. Levy-Mandel, A. Venetsanopoulos, J. Tsotsos, « Knowledge-based landmarking of cephalograms », Comput. Biomed. Res. 19 (3) (1986) 282–309.

[8] L. Mero, Z. Vassy, « A simpliffed and fast version of the Hueckel operator for finding optimal edges in pictures », Proceedings of the Fourth International Joint Conference on Artificial Intelligence, Tbilissi, Georgia, USSR, September 1975, pp. 650–655.

[9] S. Parthasaraty, S. Nugent, P.G. Gregson, D.F. Fay, « Automatic landmarking of cephalograms », Comput. Biomed. Res. 22 (1989) 248–269.

[10] C.K. Yan, A. Venetsanopoulos, E. Filleray, « An expert system for landmarking of cephalograms », Proceedings of the Sixth International Workshop on Expert Systems and Applications, 1986, pp. 337–356.

[11] J.L. Contereras-Vidal, J. Garza-Garza, « Knowledge-based system for image processing and interpolation of cephalograms », Proceedings of the Canadian Conference on Electrical and Computer Engineering, 1990, pp. 75.11–75.14.

[12] P.H. Jackson, G.C. Dickson, D.J. Birnie, Digital « image processing for cephalometric radiographic: a preliminary report », Br. J. Orthod. 12 (1985) 122

[13] A.M. Cohen, A.D. Linney, « A low cost system for computer-based cephalometric analysis », Br. J. Orthod. 13 (1986) 105–108.

[14] Forsyth D. D.Davis, « Knowledge-based cephalometric analysis: a comparison with clinicians using interactive computer methods», Comput. Biomed. Res. 27 (1994) 10–28.

[15] M. Sid-Ahmed, J. Cardillo, « An image processing system for the automatic extraction of craniofacial landmarks », IEEE Trans. Med. Imaging 13 (2) (1994) 275–289.

[16] V. Grautel, M.C. Juan, C. Monserrat, C. Knoll, « Automatic localization of cephalometric landmarks », J. Biomed. Inf. 34 (2001) 146–156.

[17] M. Desvignes, B. Romaniuk, R. Demoment, M. Revenu, M.J. Deshayes, « Computer assisted landmarking of cephalometric radiographs », Proceedings of the Fourth IEEE Southwest Symposium on Image Analysis and Interpretation, 2000, pp. 296–300.

[18] T.J. Hutton, S. Cunningham, P. Hammond, « An evaluation of active shape models for the automatic identification of cephalometric landmarks », Eur. J. Orthodont. 22 (5) (2000) 499–508.

[19] E. Uchino, T. Yamakawa, « High speed fuzzy learning machine with guarantee of global minimum and its application to chaotic system identification and medical image processing », Proceedings of the Seventh International Conference on Tools with Artificial Intelligence, 1995, pp. 242–249.

[20] A. Innes, V. Ciesielski, J. Mamutil, S. John, « Landmark detection for cephalometric radiology images using pulse coupled neural networks », International Conference in Computing in Communications, June 2002, pp. 391–396.

[21] Kragskov J, Bosch C, Gyldensted « Comparison of the reliability of craniofacial anatomic landmarks based on cephalo-metric radiographs and 3-dimensional CT scans », Cleft Palate Crani- ofac J 1997; 34:111–6.

[22] Ferrario VF, Sforza C, Poggio CE, « Facial 3-dimensional morphometry ». Am J Orthod Dentofac Orthop 1996; 109:86–93.

[23] Gwen R. J. Swennen,Filip Schutyser,Jarg-Erich Hausamen « Three-dimensional cephalometry: a color atlas and manual » Amazon Book.

[24] Milnor (j.w), « Morse theory », Princeton University Press, Princeton, NJ, (1963)

[25] Reeb, G. « Sur les points singuliers d'une forme complètement intégrable ou d'une fonction numérique ». Livre stringer (1946).

[26] Tony Tong Thése « Indexation 3D de bases de données d'objets par graphes de Reeb améliorés » (2005)

[27] Hilaga, Shigawa, « Topology Matching for fully automatic Similarity Estimation of 3D Shape », ACM SIGGRAPH, Los Angeles, CA, USA (2001).

[28] J. Tierny, J. Vandeborne et M. Daouadi, « Graphe de Reeb de haut niveau de maillages polygonaux ». Journées de l'association Francophone d'informatique graphique, bordeaux (2006).

[29] P. Cignoni, C. Montani, R. Scopigno : « A comparison of mesh simplification algorithms », Int. Symp. on 3D Data Processing, Visualization, and Transmission.

[30] Besl P.J., McKay N.D., "A Method for Registration of 3D Shapes", IEEE Trans. On Pattern Analysis and Machine Intelligence (TPAMI), Vol.14(2), pp. 239-255,1992.

[31] F. L. Bookstein, "Principal Warps: Thin-Plate Splines and the Decomposition of Deformations" IEEE Transaction on pattern analysis and machine intelligence. Vol 11, No 6, June 1989.

[32] Makram Mestiri, Sami Bourouis and Kamel Hamrouni, "Automatic Mesh Segmentation using atlas projection and thin plate spline: Application for a Segmentation of Skull Ossicles", VISAPP 2011.